RSC Advances

PAPER

View Article Online
View Journal | View Issue

Cite this: *RSC Adv.*, 2022, **12**, 17944

A large negative magnetoresistance effect in semiconducting crystals composed of an octahedrally ligated phthalocyanine complex with high-spin manganese(III)†

Kosuke Mine,[a] Masayuki Yamaguchi,[a] Hiroshi Murakawa,[b] Noriaki Hanasaki[b] and Masaki Matsuda *[a]

A design for an octahedrally ligated phthalocyanine complex with high-spin manganese(III) ($S = 2$) and $Mn^{III}(Pc)Cl_2$ (Pc = phthalocyanine) is presented. The presence of high-spin state Mn^{III} in the fabricated $Ph_4P[Mn^{III}(Pc)Cl_2]_2$ (Ph_4P = tetraphenylphosphonium) semiconducting molecular crystal is indicated by the Mn–Cl distance, which suggests an electronic configuration of $(d_{yz})^2(d_{zx})^2(d_{xy})^1(d_{z^2})^1$. This was confirmed by the Curie constant ($C = 5.69$ emu K mol^{-1}), which was found to be significantly larger than that of the isostructural $Ph_4P[Mn^{III}(Pc)(CN)_2]_2$, where Mn^{III} adopts a low-spin state ($S = 1$). The magnetoresistance (MR) effects of $Ph_4P[Mn^{III}(Pc)Cl_2]_2$ at 26.5 K under 9 T static magnetic fields perpendicular and parallel to the *c*-axis were determined to be −30% and −20%, respectively, which are significantly larger values than those of $Ph_4P[Mn^{III}(Pc)(CN)_2]_2$. Furthermore, the negative MR effect is comparable to that of $Ph_4P[Fe^{III}(Pc)(CN)_2]_2$ ($S = 1/2$), which exhibits the largest negative MR effect reported for $[M^{III}(Mc)L_2]$-based systems (Mc = macrocyclic ligand, L = axial ligand). This suggests that the spin state of the metal ion is the key to tuning the MR effect.

Received 10th January 2022
Accepted 12th June 2022

DOI: 10.1039/d2ra00188h

rsc.li/rsc-advances

Introduction

Molecular spintronics, which is the concept of spintronics based on molecular compounds, has attracted significant interest in recent years,[1] wherein the magnetoresistance (MR) effect is a typical phenomenon of note. In molecular systems, the magnetic interaction between π-conduction electrons and the local spin is crucial to ensure a correlation between the electrical conductance and the magnetism. In this regard, metal complexes comprised of phthalocyanine (M(Pc)) and its derivatives, where the d-spin of the central metal ion is surrounded by a π-conjugated macrocyclic ligand, are attractive systems. For example, molecular semiconducting crystals have been constructed using $[Fe^{III}(Pc)L_2]$ units (L is an axial ligand),[2–5] where Fe^{III} adopts a low-spin state ($S = 1/2$).

In an $[Fe^{III}(Pc)L_2]$ unit, the highest occupied molecular orbital (HOMO) is the π-orbital of Pc, and the next HOMOs contain the degenerated d_{yz} and d_{zx} orbitals where d-spin exists. Thus, molecular semiconducting crystals, which are mixed-valence compounds composed of the $[Fe^{III}(Pc)L_2]$ unit, exhibit large negative MR effects irrespective of the crystal structure.[4–7] Although the reported systems were initially expected to possess a 3/4-filled HOMO band, semiconducting behavior caused by the charge-ordered state of the π-conduction electrons has been observed with antiferromagnetic interaction between the d-spins. In the 3/4-filled system, the introduction of antiferromagnetic ordered d-spins means that the insulating state resulting from the charge-ordered state of the π-conduction electrons is stabilized *via* the intramolecular π–d interaction,[8,9] *i.e.*, the magnetic interaction between the π-conduction electrons and the d-spin. It is therefore believed that the large negative MR effects of molecular semiconducting crystals consisting of $Fe(Pc)L_2$ emerge from the suppression of the charge-ordered state of π-conduction electrons by an external magnetic field, which disturbs the antiferromagnetic order of the d-spins.[10,11] Furthermore, the MR effect can be tuned through the molecular design, such as the substitution of a macrocyclic ligand,[12,13] axial ligands,[5] or a central metal ion.[14–17]

Among the reported systems, the MR ratio of $Ph_4P[Fe(Pc)(CN)_2]_2$ (Ph_4P = tetraphenylphosphonium) was determined to be −99% at 20 K under a 38 T magnetic field.[7] When the central metal ion was substituted to give $Ph_4P[Mn^{III}(Pc)(CN)_2]_2$, where Mn^{III} adopted the low-spin state ($S = 1$), the MR effect was significantly smaller than those of isostructural $Fe^{III}(Pc)L_2$-based systems.[4–7,16] However, it has been

[a]*Department of Chemistry, Kumamoto University, 2-39-1 Kurokami, Chuo-ku, Kumamoto, 860-8555, Japan. E-mail: masaki@kumamoto-u.ac.jp*

[b]*Department of Physics, Osaka University, 1-1 Machikaneyama, Toyonaka, Osaka, 560-0043, Japan*

† CCDC 2129804 for $Ph_4P[Mn(Pc)Cl_2]_2$. For crystallographic data in CIF or other electronic format see **https://doi.org/10.1039/d2ra00188h**

shown that not only the kind of the element but also the spin state of the central metal ion significantly affects the MR effect. For example, despite the significantly weaker antiferromagnetic interaction, the MR effect of $Ph_4P[Fe^{III}(tbp)Br_2]_2$ (tbp = tetrabenzoporphyrin) is similar to that of the isostructural $Ph_4P[Fe^{III}(tbp)(CN)_2]_2$, where the spin state of Fe^{III} is the high-spin state ($S = 5/2$) in the former and the low-spin state in the latter.[12,18] For the purpose of the current study, we chose to focus on the spin states of the Mn^{III} ion. It is rare for Mn^{III} to adopt a low-spin state,[19] and a very strong ligand field is required to induce it.[19,20] Therefore, we anticipated that it could be possible to fabricate a $Ph_4P[Mn^{III}(Pc)L_2]_2$ molecular semiconducting crystal where Mn^{III} adopts a high-spin state ($S = 2$) by substituting the strong CN ligand with a weaker ligand, such as Cl. Changing the spin state of Mn^{III} would be expected to induce drastic changes in the electrical and magnetic properties of the resulting system.

The spin state of a metal ion in a coordination complex is the key to determining its functionality. For example, heme proteins consisting of iron porphyrin change their functionality when the valence and spin states of iron are altered.[21,22] Because their molecular structures resemble heme, metal complexes based on porphyrin and its derivatives, including phthalocyanines, have been widely studied as biomimetic models,[23] and various high-spin Mn^{III} complexes with porphyrin or phthalocyanine moieties have been reported.[24,25] Prior to the current study, the Gaussian 16 software package[26] was used to perform theoretical calculations for a $[Mn^{III}(Pc)L_2]$ (L = Cl or CN) unit using the density functional theory (DFT) approach at the B3LYP/6-311G(d) level of theory. The geometry optimization results under D_{2h} symmetry for $Mn^{III}(Pc)L_2$ are shown in Table 1. As indicated, compared with the results for L = CN systems, where the low-spin state is evidently more stable than the high-spin state, the differences between the free energies of the low- and high-spin states of Mn^{III} are relatively small for both $Mn^{III}(Pc)Cl_2$ and $[Mn^{III}(Pc)Cl_2]^-$, where Pc is the open shell (oxidized) and the closed shell (not oxidized), respectively. Owing to this small difference in the calculated free energies, we anticipated a possibility that Mn^{III} in the $Mn^{III}(Pc)Cl_2$-based mixed-valence compounds would adopt a high-spin state.

Thus, in this study, a semiconducting mixed-valence crystal of $Ph_4P[Mn^{III}(Pc)Cl_2]_2$ is synthesized, and the high-spin state of Mn^{III} is confirmed. Its molecular and crystal structure, magnetic and electrical transport properties, and MR effect are reported. Notably, this is the first study investigating the effects of changing the spin state of the Mn^{III} center on the electrical transport properties of the resulting system.

Table 1 Summary of the optimized geometries of $Mn^{III}(Pc)L_2$ and $[Mn^{III}(Pc)L_2]^-$ under D_{2h} symmetry from DFT calculations

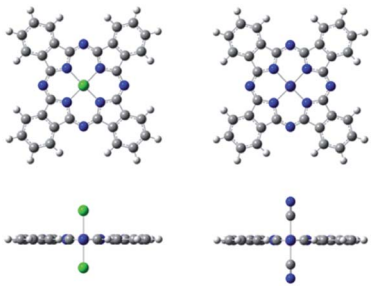

	$Mn(Pc)Cl_2$		$Mn(Pc)(CN)_2$	
	Quartet	Sextet	Quartet	Sextet
Relative free energy (kcal mol^{-1})	0	+8.3	0	+19.2
Mn–N (Å)	1.969	1.979	1.968	2.039
Mn–N (Å)	1.969	1.980	1.968	2.039
Mn–L (Å)	2.269	2.510	2.015	2.036
	$[Mn(Pc)Cl_2]^-$		$[Mn(Pc)(CN)_2]^-$	
	Triplet	Quintet	Triplet	Quintet
Relative free energy (kcal mol^{-1})	0	+0.7	0	+12.6
Mn–N (Å)	1.980	1.985	1.977	2.046
Mn–N (Å)	1.981	1.985	1.978	2.047
Mn–L (Å)	2.316	2.560	2.032	2.044

Results and discussion

Molecular and crystal structure

The crystal structure and crystal data of $Ph_4P[Mn^{III}(Pc)Cl_2]_2$ are given in Fig. 1 and Table 2, respectively. As in the cases of $Ph_4P[Fe^{III}(Pc)L_2]_2$ (Fe^{III}: d^5, $S = 1/2$) and $Ph_4P[Co^{III}(Pc)L_2]_2$ (Co^{III}: d^6, $S = 0$) (L = CN, Cl, or Br), the substitution of axial ligands has little influence on the molecular arrangement. Therefore, $Ph_4P[Mn^{III}(Pc)Cl_2]_2$, which possesses a tetragonal unit cell with a $P4_2/n$ space group, is isostructural to $Ph_4P[Mn^{III}(Pc)(CN)_2]_2$.[16] The 1 : 2 ratio of cation:$[Mn(Pc)Cl_2]$ units indicates that an average of one electron is oxidized for every two $[Mn(Pc)Cl_2]$ units. This

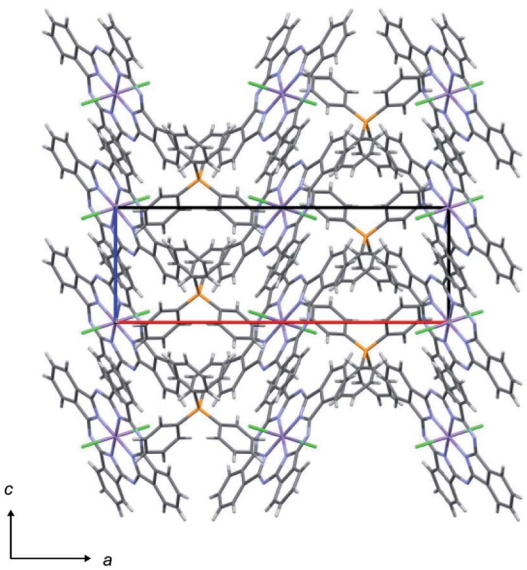

Fig. 1 Crystal structure of $Ph_4P[Mn^{III}(Pc)Cl_2]_2$ viewed along the *b*-axis. Some molecules have been omitted for clarity.

Table 2 Crystal data and structure refinement results for $Ph_4P[Mn(Pc)Cl_2]_2$

CCDC number	2129804
Chemical formula	$C_{88}H_{52}Cl_{14}Mn_2N_{16}P$
Formula weight	1616.10
Crystal description	Black needle
T (K)	293
Crystal system	Tetragonal
Space group	$P4_2/n$
a (Å)	21.6778 (4)
c (Å)	7.4426 (2)
V (Å^3)	3497.48 (4)
Z	2
d_{cal} (g cm^{-3})	1.535
Radiation	MoKα
Wavelength (Å)	0.71073
μ (mm^{-1})	0.602
No. of measured reflections	17 320
No. of independent reflection	3679
No. of observed reflections	2564 ($I > 2\sigma(I)$)
R ($I > 2\sigma(I)$)	$R_1 = 0.0420$ $wR_2 = 0.1402$
Goodness-of-fit	0.931
Parameters	252

means that the one-dimensional regular chains of $[Mn(Pc)Cl_2]$ units overlapping two peripheral benzene rings along the c-axis form a one-dimensional electronic system with a 3/4-filled HOMO band. The interplanar distances between benzene rings are 3.47 and 3.40 Å, which are similar to those for $Ph_4P[Mn^{III}(Pc)(CN)_2]_2$ (*i.e.*, 3.47 and 3.41 Å). Using the extended Hückel calculation,‡ the overlap integral between the HOMOs of Pc in $Ph_4P[Mn^{III}(Pc)Cl_2]_2$ was estimated to be 9.3×10^{-3}, which is slightly larger than that of $Ph_4P[Mn^{III}(Pc)(CN)_2]_2$ (9.0×10^{-3}), thereby indicating that substitution of the axial ligands has little effect on conduction path formation.

With respect to the bond length, theoretical calculations predicted that the Mn–Cl distance would be notably larger for high-spin Mn^{III} than for low-spin Mn^{III}, and that the Mn–N distances would be insensitive to the Mn^{III} spin state (Table 1). This suggests that the electronic configuration of Mn^{III} in the high-spin state is $(d_{yz}, d_{zx})^2(d_{xy})^1(d_{z^2})^1$, as reported for porphyrin complexes,[27,28] and that in the low-spin state is $(d_{xy})^2(d_{yz}, d_{zx})^2$.[19] The fact that the former possesses occupied d_{z^2} renders the Mn–Cl distance larger in the high-spin Mn^{III} complex. In contrast, since $d_{x^2-y^2}$ is unoccupied in both spin states, the Mn–N distance is approximately the same. The observed Mn–Cl distance of 2.555 Å is consistent with the predicted value for a $[Mn(Pc)Cl_2]$ unit with high-spin Mn^{III}.

Therefore, it can be concluded that the Mn^{III} center in the obtained $Ph_4P[Mn(Pc)Cl_2]_2$ adopts a high-spin state.

Magnetic susceptibility

Fig. 2 shows the temperature dependence of the magnetic susceptibility χ_p of $Ph_4P[Mn^{III}(Pc)Cl_2]_2$ under a static magnetic field of 1 T. For temperatures greater than 20 K, the χ_p *vs.* T plot obeys the Curie–Weiss law with a Curie constant of $C = 5.69$ emu K mol^{-1} and a Weiss temperature of $\theta = -2.4$ K. This Curie constant is significantly larger than that reported for $Ph_4P[Mn^{III}(Pc)(CN)_2]_2$, where Mn^{III} adopts the low-spin state ($S = 1$) ($C = 3.01$ emu K mol^{-1}).[16] It is therefore apparent that the Mn^{III} center in $Ph_4P[Mn(Pc)Cl_2]_2$ adopts the high-spin state ($S = 2$) as expected, although the observed Curie constant of $C = 5.69$ emu K mol^{-1} is smaller than the predicted value of 6.00 emu K mol^{-1} under the assumption of $S = 2$ and $g = 2$.

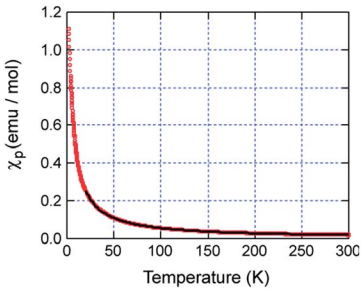

Fig. 2 Temperature dependence of the magnetic susceptibility χ_p for the formula unit $Ph_4P[Mn^{III}(Pc)Cl_2]_2$ under a static magnetic field of 1 T. The solid line is the best fit to the Curie–Weiss law with the parameters $C = 5.69$ emu K mol^{-1} and $\theta = -2.4$ K.

The negative Weiss temperature indicates that there is an antiferromagnetic interaction between the d-spins of high-spin Mn^{III}. Antiferromagnetic interactions between d-spins are common in the low-spin Fe^{III} and Mn^{III} complexes $Ph_4P[Fe(Pc)L_2]_2$,[2–5] $Ph_4P[Fe(tbp)(CN)_2]_2$,[12] and $Ph_4P[Mn(Pc)(CN)_2]_2$,[16] and the high-spin Fe^{III} complex $Ph_4P[Fe(tbp)Br_2]_2$.[18] According to the mean-field approximation, the Weiss temperature can be expressed as $\theta = 2zJ_{dd}S(S+1)/3\,k_B$, where z, J_{dd}, and k_B are the number of nearest neighbors, an intermolecular magnetic exchange interaction between the d-spins, and the Boltzmann constant, respectively. As summarized in Table 3, the absolute value $|J_{dd}|$ for $Ph_4P[Mn^{III}(Pc)Cl_2]_2$ is less than that for $Ph_4P[Mn^{III}(Pc)(CN)_2]_2$, indicating that substituting the CN axial ligands with Cl weakens the antiferromagnetic interaction.

Electrical resistance measurements

Fig. 3 shows the temperature dependence of the electrical resistivities of $Ph_4P[Mn^{III}(Pc)Cl_2]_2$ and $Ph_4P[Mn^{III}(Pc)(CN)_2]_2$ along their c-axes. Despite the 3/4-filled HOMO band, semiconducting behavior was observed. Such behavior is exhibited by all $Ph_4P[M^{III}(Mc)L_2]_2$ systems (Mc = macrocyclic ligand) and has been attributed to the fluctuations in the charge-ordered state of the π-conduction electrons.[29] The electrical resistivity of $Ph_4P[Mn^{III}(Pc)Cl_2]_2$ at room temperature (~25 °C) is approximately 5 Ω cm, which is one order of magnitude higher than that of $Ph_4P[Mn^{III}(Pc)(CN)_2]_2$. Furthermore, the activation energy of $Ph_4P[Mn^{III}(Pc)Cl_2]_2$ in the temperature range of 25–300 K was estimated to be 34 meV, which is significantly larger than that of $Ph_4P[Mn^{III}(Pc)(CN)_2]_2$ (8.4 meV at <70 K).[16] This suggests that the charge-ordered state of the π-conduction electrons in $Ph_4P[Mn^{III}(Pc)Cl_2]_2$ is more developed than in the

‡ Calculations were performed using the CAESAR 2.0 software package (PrimeColor Software, Inc). Default parameters were used.

Table 3 Spin of the d electron (S), the Weiss temperature (θ), the exchange constant (J_{dd}), and the MR effect of select $Ph_4P[M^{III}(Mc)L_2]_2$ systems

	$Ph_4P[Mn(Pc)Cl_2]_2$	$Ph_4P[Mn(Pc)(CN)_2]_2$	$Ph_4P[Fe(tbp)Br_2]_2$	$Ph_4P[Fe(tbp)(CN)_2]_2$	$Ph_4P[Fe(Pc)(CN)_2]_2$
S	2	1	5/2	1/2	1/2
θ	−2.4 K	−3.1 K	−2.5 K	−8.0 K	−12 K
J_{dd}/k_B	−0.30 K	−1.16 K	−0.21 K	−8.0 K	−12.0 K
MR effect under 9 T at 30 K	−25% ($B\perp c$) −18% ($B//c$)	N/A[a]	−6% ($B\perp c$) −8% ($B//c$)	−14% ($B\perp c$) −9% ($B//c$)	−30% ($B\perp c$) −18% ($B//c$)
Reference	This study	16	18	12	6

[a] The MR effect at 10.7 K under a 8 T magnetic field is reported to be −8.7%. ⊥ and//indicate perpendicular and parallel alignments, respectively.

case of $Ph_4P[Mn^{III}(Pc)(CN)_2]_2$. As mentioned above, the charge-ordered state of the π-conduction electrons is stabilized by the antiferromagnetic interaction between the d-spins and the intramolecular π–d interaction. Therefore, the intramolecular π–d interaction in the high-spin $Ph_4P[Mn^{III}(Pc)Cl_2]_2$ system is believed to be stronger than that in the low-spin $Ph_4P[Mn^{III}(Pc)(CN)_2]_2$ system. A likely cause of the change in the π–d interaction is the change in the electronic structure resulting from the substitution of the axial ligands. The development of the charge-ordered state in $Ph_4P[Mn^{III}(Pc)Cl_2]_2$ therefore indicates that the negative MR effect is expected to be larger than that of $Ph_4P[Mn^{III}(Pc)(CN)_2]_2$.

Magnetoresistance measurements

Fig. 4(a) and (b) show the relationships between the electrical resistance of $Ph_4P[Mn^{III}(Pc)Cl_2]_2$ and the magnetic fields perpendicular and parallel to the c-axis, respectively. In both cases, a large negative MR effect was observed, which increased as the magnetic field increased or the temperature decreased. At 26.5 K, the MR effect under a 8 T magnetic field perpendicular to the c-axis was −24%, and that under the same field parallel to the c-axis was −17%. These values are significantly larger than the MR effect reported for $Ph_4P[Mn^{III}(Pc)(CN)_2]_2$ (−8.7% at 10.7 K, under a 8 T magnetic field).[16] Table 3 summarizes spins of the d electrons, J_{dd}, and the MR effects for $Ph_4P[Mn^{III}(Pc)Cl_2]_2$, $Ph_4P[Mn^{III}(Pc)(CN)_2]_2$, $Ph_4P[Fe^{III}(tbp)Br_2]_2$, $Ph_4P[Fe^{III}(tbp)(CN)_2]_2$, and $Ph_4P[Fe^{III}(Pc)(CN)_2]_2$. As for the isostructural $Ph_4P[Fe(Mc)L_2]_2$ with low-spin Fe^{III} ($S = 1/2$), the negative MR effect reduces as $|J_{dd}|$ decreases.[5,6,12] Therefore, it is notable that a significantly larger negative MR effect was observed for the high-spin $Ph_4P[Mn^{III}(Pc)Cl_2]_2$ system than for the low-spin $Ph_4P[Mn^{III}(Pc)(CN)_2]_2$ system, despite the fact that $|J_{dd}|$ is smaller for $Ph_4P[Mn^{III}(Pc)Cl_2]_2$. A similar trend was observed for $Ph_4P[Fe^{III}(tbp)Br_2]_2$ with high-spin Fe^{III} and $Ph_4P[Fe^{III}(tbp)(CN)_2]_2$ with low-spin Fe^{III}, and the negative MR effect for $Ph_4P[Fe(tbp)Br_2]_2$ was found to be similar to that of $Ph_4P[Fe^{III}(tbp)(CN)_2]_2$, despite the fact that $|J_{dd}|$ is significantly smaller for $Ph_4P[Fe^{III}(tbp)Br_2]_2$. Considering the mechanism of the negative MR effect, the fact that high-spin systems with a small $|J_{dd}|$ exhibited negative MR effects larger than or similar to those of low-spin systems implies that the high-spin systems possess stronger intramolecular π–d interactions than the low-spin systems. These results suggest that the high-spin state of M^{III} in the $[M(Mc)L_2]$ unit aids the emergence of the negative MR effect. The MR effects of $Ph_4P[Mn^{III}(Pc)Cl_2]_2$ at 30 K under 9 T magnetic fields perpendicular and parallel to the c-axis are −25% and −18%, respectively. These values are comparable to those of $Ph_4P[Fe^{III}(Pc)(CN)_2]_2$, which exhibits the largest MR effect reported in $[M(Mc)L_2]$-based systems.

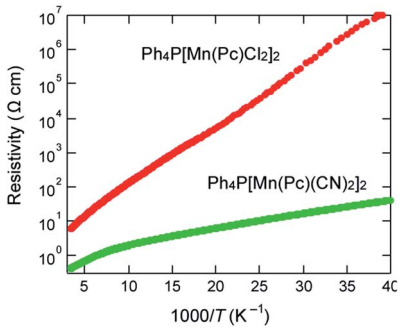

Fig. 3 Temperature dependence of the electrical resistivity along the c-axes of $Ph_4P[Mn^{III}(Pc)Cl_2]_2$ (red) and $Ph_4P[Mn^{III}(Pc)(CN)_2]_2$ (green).

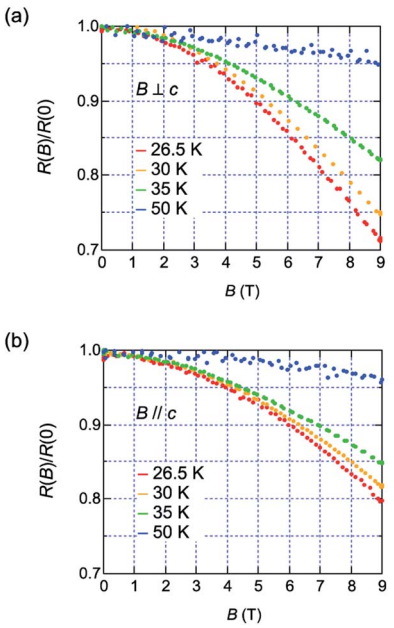

Fig. 4 Resistance under the magnetic fields (a) perpendicular and (b) parallel to the c-axis at various temperatures. The resistance values are normalized to the corresponding resistance under a zero magnetic field.

Conclusions

Based on the density functional theory calculations, a $Ph_4P[Mn^{III}(Pc)Cl_2]_2$ semiconducting molecular crystal where the octahedrally ligated Mn^{III} adopts a high-spin state ($S = 2$) was designed and fabricated. Although the intermolecular magnetic interaction J_{dd} between the Mn^{III} ions was estimated to be -0.30 K, and the absolute value was smaller than that of the isostructural $Ph_4P[Mn^{III}(Pc)(CN)_2]_2$ with low-spin Mn^{III} ($S = 1$, $J_{dd} = -1.16$ K), a large negative magnetoresistance (MR) effect was observed. The MR effects at 26.5 K under 9 T magnetic fields perpendicular and parallel to the *c*-axis were -30% and -20%, respectively. These MR effects are significantly larger than those observed for the low-spin $Ph_4P[Mn^{III}(Pc)(CN)_2]_2$ system, and are similar to those of $Ph_4P[Fe^{III}(Pc)(CN)_2]_2$, which exhibited the largest MR effect among previously reported $[M^{III}(Mc)L_2]$-based semiconducting crystals. Therefore, this study revealed that the spin state of the metal ion is the key to tuning the MR effect, and the high-spin state aids the emergence of a large negative MR effect. Further research into $[M^{III}(Mc)L_2]_2$-based systems, where M^{III} adopts a high-spin state, would benefit the development of molecular spintronics.

Experimental details

Synthetic procedures

Mn(Pc) was synthesized according to the procedure described by Rutter and McQueen,[30] using quinoline as a solvent instead of 1,2-propanediol. The obtained Mn(Pc) (6 mg, 0.01 mmol) was electrochemically oxidized in a mixed solution of DMF:acetone (8 mL, 1 : 1 v/v, super dehydrated grade, used as purchased from FUJIFILM Wako Chemicals) containing $Ph_4P{\cdot}Cl$ (24 mg, 0.06 mmol, used as purchased from Tokyo Chemical Industry) at 25 °C using an electrocrystallization cell under an Ar atmosphere. The cell was equipped with a glass frit between the two compartments. A constant current of 0.6–1.0 μA was passed between two platinum electrodes immersed in the solutions in each compartment for 2–3 weeks. Black needle-like crystals of $Ph_4P[Mn^{III}(Pc)Cl_2]_2$ grew on the anode surface and were harvested by filtration.

Crystal structure determination

Crystal data for $Ph_4P[Mn^{III}(Pc)Cl_2]_2$ were collected at 293 K using an automated Rigaku SuperNova system with monochromated Mo Kα radiation ($\lambda = 0.71073$ Å). The structure was solved using a direct method with SHELXT-2014/5 (ref. 31) and refined using a full-matrix least-squares technique with SHELXL-2018/1.[32] Anisotropic and isotropic thermal parameters were employed for non-hydrogen and hydrogen atoms, respectively.†

Measurements

The electrical resistivity along the *c*-axis of a $Ph_4P[Mn^{III}(Pc)Cl_2]_2$ single crystal was measured using a physical property measurement system (PPMS) from Quantum Design with a static magnetic field of up to 9 T over a temperature range of 25–300 K. Gold wires were attached to the sample using gold paste once gold deposition was complete. In the high-temperature region, where the resistance was less than 10^7 Ω, the standard four-probe method was adopted; in the low-temperature region, where the resistance was greater than 10^6 Ω, the two-probe method was applied. Static magnetic susceptibility measurements were obtained using a Quantum Design magnetic property measurement system (MPMS) superconducting quantum interference device (SQUID) with a 1 T magnetic field over the temperature range of 2–300 K.

Conflicts of interest

There are no conflicts to declare.

Acknowledgements

This study was supported in part by a Grant-in-Aid for Scientific Research (B) (No 19H02691) from the Japan Society for the Promotion of Science. The authors are grateful for the support by the Cooperative Research Program of "New Joint Research Center for Materials and Devices". We also thank Prof Akira Yoshiasa at Kumamoto University for his help with the X-ray diffraction measurements.

Notes and references

1 E. Coronado and M. Yamashita, *Dalton Trans.*, 2016, **45**, 16553–16555.
2 M. Matsuda, T. Naito, T. Inabe, N. Hanasaki, H. Tajima, T. Otsuka, K. Awaga, B. Narymbetov and H. Kobayashi, *J. Mater. Chem.*, 2000, **10**, 631–636.
3 M. Matsuda, T. Naito, T. Inabe, N. Hanasaki and H. Tajima, *J. Mater. Chem.*, 2001, **11**, 2493–2497.
4 M. Matsuda, T. Asari, T. Naito, T. Inabe, N. Hanasaki and H. Tajima, *Bull. Chem. Soc. Jpn.*, 2003, **76**, 1935–1940.
5 D. E. C. Yu, M. Matsuda, H. Tajima, A. Kikuchi, T. Taketsugu, N. Hanasaki, T. Naito and T. Inabe, *J. Mater. Chem.*, 2009, **19**, 718–723.
6 N. Hanasaki, H. Tajima, M. Matsuda, T. Naito and T. Inabe, *Phys. Rev. B*, 2000, **62**, 5839–5842.
7 N. Hanasaki, M. Matsuda, H. Tajima, E. Ohmichi, T. Osada, T. Naito and T. Inabe, *J. Phys. Soc. Jpn.*, 2006, **75**, 033703.
8 C. Hotta, M. Ogata and H. Fukuyama, *Phys. Rev. Lett.*, 2005, **95**, 216402.
9 Y. Otsuka, H. Seo and Y. Motome, *Phys. B*, 2010, **405**, S317–S320.
10 C. Hotta, *Phys. Rev. B*, 2010, **81**, 245104.
11 H. Murakawa, A. Kanda, M. Ikeda, M. Matsuda and N. Hanasaki, *Phys. Rev. B*, 2015, **92**, 054429.
12 M. Nishi, M. Ikeda, A. Kanda, N. Hanasaki, N. Hoshino, T. Akutagawa and M. Matsuda, *Dalton Trans.*, 2016, **45**, 16604–16609.
13 M. Yamaguchi, S. Iwamura, K. Mine, H. Murakawa, N. Hanasaki and M. Matsuda, *Dalton Trans.*, 2021, **50**, 5789–5794.

14 Y. Takita, H. Hasegawa, Y. Takahashi, J. Harada, A. Kanda, N. Hanasaki and T. Inabe, *J. Porphyrins Phthalocyanines*, 2014, **18**, 814–823.
15 M. Ikeda, T. Kida, T. Tahara, H. Murakawa, M. Nishi, M. Matsuda, M. Hagiwara, T. Inabe and N. Hanasaki, *J. Phys. Soc. Jpn.*, 2016, **85**, 064713.
16 M. Matsuda, G. Yoshida, J.-i. Yamaura, T. Inabe and H. Tajima, *Dalton Trans.*, 2017, **46**, 1892–1897.
17 M. Ikeda, A. Kanda, H. Murakawa, M. Matsuda, T. Inabe, H. Tajima and N. Hanasaki, *J. Phys. Soc. Jpn.*, 2016, **85**, 024713.
18 M. Nishi, R. Ishii, M. Ikeda, N. Hanasaki, N. Hoshino, T. Akutagawa, M. Sumimoto and M. Matsuda, *Dalton Trans.*, 2018, **47**, 4070–4075.
19 A. P. Hansen and H. M. Goff, *Inorg. Chem.*, 1984, **23**, 4519–4525.
20 M. Matsuda, J.-i. Yamaura, H. Tajima and T. Inabe, *Chem. Lett.*, 2005, **34**, 1524–1525.
21 H. Chen, M. I. Saito and S. Shaik, *J. Am. Chem. Soc.*, 2008, **130**, 14778–14790.
22 Y. Nakahara, K. Kimura and H. Inokuchi, *Chem. Phys. Lett.*, 1977, **47**, 251–254.
23 J. P. Collman, R. Boulatov, C. J. Sunderland and L. Fu, *Chem. Rev.*, 2004, **104**, 561–588.
24 L. J. Boucher, *Coord. Chem. Rev.*, 1972, **7**, 289–329.
25 A. B. P. Lever, *J. Chem. Soc.*, 1965, 1821–1829.
26 M. J. Frisch, G. W. Trucks, H. B. Schlegel, G. E. Scuseria, M. A. Robb, J. R. Cheeseman, G. Scalmani, V. Barone, G. A. Petersson, H. Nakatsuji, X. Li, M. Caricato, A. V. Marenich, J. Bloino, B. G. Janesko, R. Gomperts, B. Mennucci, H. P. Hratchian, J. V. Ortiz, A. F. Izmaylov, J. L. Sonnenberg, D. Williams-Young, F. Ding, F. Lipparini, F. Egidi, J. Goings, B. Peng, A. Petrone, T. Henderson, D. Ranasinghe, V. G. Zakrzewski, J. Gao, N. Rega, G. Zheng, W. Liang, M. Hada, M. Ehara, K. Toyota, R. Fukuda, J. Hasegawa, M. Ishida, T. Nakajima, Y. Honda, O. Kitao, H. Nakai, T. Vreven, K. Throssell, J. A. Montgomery, Jr., J. E. Peralta, F. Ogliaro, M. J. Bearpark, J. J. Heyd, E. N. Brothers, K. N. Kudin, V. N. Staroverov, T. A. Keith, R. Kobayashi, J. Normand, K. Raghavachari, A. P. Rendell, J. C. Burant, S. S. Iyengar, J. Tomasi, M. Cossi, J. M. Millam, M. Klene, C. Adamo, R. Cammi, J. W. Ochterski, R. L. Martin, K. Morokuma, O. Farkas, J. B. Foresman and D. J. Fox, *Gaussian 16, Revision A.03*, Gaussian, Inc., Wallingford CT, 2016.
27 C. L. Hill and M. M. Willamson, *Inorg. Chem.*, 1985, **24**, 2836–2841.
28 M. G. I. Galinato, E. P. Brocious, F. Paulat, S. Martin, J. Skodack, J. B. Harland and N. Lehnert, *Inorg. Chem.*, 2020, **59**, 2144–2162.
29 N. Hanasaki, K. Masuda, K. Kodama, M. Matsuda, H. Tajima, J. Yamazaki, M. Takigawa, J.-i. Yamaura, E. Ohmichi, T. Osada, T. Naito and T. Inabe, *J. Phys. Soc. Jpn.*, 2006, **75**, 104713.
30 H. A. Rutter, Jr. and J. D. McQueen, *J. Inorg. Nucl. Chem.*, 1960, **12**, 361–363.
31 G. M. Sheldrick, *Acta Crystallogr., Sect. A: Found. Adv.*, 2015, **71**, 3–8.
32 G. M. Sheldrick, *Acta Crystallogr., Sect. C: Struct. Chem.*, 2015, **71**, 3–8.